Raman Characterization and Polarity Tuning of Aligned Single-Walled Carbon Nanotubes on Quartz

Bo Lei, Koungmin Ryu, Lewis Gomez De-Arco, Song Han[1], Alexander Badmaev, Damon Farmer[2], Kevin Kim[2], Roy Gordon[2], Kang L. Wang[1], and Chongwu Zhou*

Department of Electrical Engineering–Electrophysics, University of Southern California, Los Angeles, CA 90089, U.S.A.
[1]*Department of Electrical Engineering, University of California at Los Angeles, Los Angeles, CA 94035, U.S.A.*
[2]*Department of Chemistry and Chemical Biology Cambridge, Harvard University, Cambridge, MA 02138, U.S.A.*

Received July 24, 2009; revised October 13, 2009; accepted October 18, 2009; published online February 22, 2010

Raman characterization has been employed to study key features of highly aligned single-walled carbon nanotubes grown on quartz substrates. The nanotubes are observed to possess an estimated metallic/semiconducting ratio of 1 : 2.7, and Raman spectra also confirm the high integrity of nanotubes before and after being transferred from quartz to Si/SiO_2 substrates. Based on the as-grown and the transferred aligned nanotubes, we have further fabricated top- and back-gated nanotube devices, respectively. The top-gated transistors exhibit ambipolar transport characteristics with high transconductance, small subthreshold swing of 110 mV/decade and on/off ratio of 10^7, while the back-gated transistors show unipolar p-type characteristics. Furthermore, we have demonstrated polarity tuning to produce both predominately n- and p-type top-gated carbon nanotube transistors by controlling the polarity of gate voltage during electrical breakdown, which has great potential for building complementary carbon nanotube circuits.

DOI: 10.1143/JJAP.49.02BC02

1. Introduction

Since discovered by Ijima in 1991,[1)] single-walled carbon nanotubes (SWNTs) have been intensively studied owing to their unique structural, mechanical and electronic properties promising for many potential applications.[2)] In particular, high carrier mobility and native small dimension of SWNTs render them to be a good candidate for nanoelectronics. Recently, based on multiple and parallel nanotube arrays on sapphire[3–5)] or quartz,[6–8)] Liu *et al.*[9)] and Kang *et al.*[10)] have produced high performance carbon nanotube devices, making a significant advance toward large-scale nanotube electronics. Furthermore, the full wafer-scale integrated nanotube circuits[11)] using the aligned transferred nanotube arrays were successfully demonstrated by our group. Specifically, the aligned nanotube approach offers several advantages over the traditional nanotube approach using randomly grown nanotubes on Si/SiO_2 substrates, including registration free process, minimized parasitic capacitance, and less cross-talking between nanotubes.[12)] However, previous studies uncovered some important aspects of highly aligned single-walled carbon nanotubes on quartz, such as metallic/semiconducting ratio and the integrity of nanotubes before and after transfer, although aligned nanotubes are expected to have better structural/electronic uniformity along the nanotubes than unaligned nanotubes, namely, less chance of producing chirality change or intermolecular junction/kink in a nanotube. In addition, there are two important technological components to be achieved for advanced complementary metal–oxide–semiconductor (CMOS) integrated nanotube circuits such as ring-oscillators, decoders, and shifters. One is the practical way to get both n- and p-type transistors and the other is the metallic nanotube removal to achieve high on/off ratio.

In this paper, extensive Raman characterization of the highly aligned nanotubes on quartz revealed the polarization of Raman spectra, the metallic/semiconducting nanotube ratio, and the defect density. Based on the aligned nanotubes and the transferred nanotubes, we fabricated nanotube transistors with top-gate and back-gate, respectively. Furthermore, we demonstrate a way to controllably obtain either predominantly n- or p-type nanotube transistors by controlling the gate voltage polarity during electrical breakdown. Transistors made by this approach may lead to their integration into large-scale CMOS circuits.

2. Experiment and Results

Both aligned nanotubes on quartz and unaligned nanotubes on Si/SiO_2 are grown on patterned Fe catalyst[13)] by conventional chemical vapor deposition (CVD) method.[14)] Briefly, the substrates were first cleaned with acetone and isopropanol, photolithography was then used to open windows on the substrates followed by catalyst deposition using thermal evaporation. After removal of the photoresistor, the samples were calcinated at 900 °C for 10 min in air to form oxidized catalyst islands at controlled positions. Finally, the nanotubes were grown with the gas flow of C_2H_4 (10 sccm), CH_4 (2500 sccm), and H_2 (600 sccm) at 900 °C for 10 min.

With these nanotubes, we performed the detailed characterization in terms of diameter distribution and Raman analysis of polarization, defects and metallic/semiconducting nanotube ratio. Figure 1(a) shows scanning electron microscopy (SEM) image of the aligned nanotubes with source and drain metal contacts, which also function as alignment marks to facilitate the Raman studies. Before defining the metal contacts, we used atomic force microscopy (AFM) to scan the aligned nanotube samples. Figure 1(b) shows a histogram of nanotube diameter distribution outside the region of catalyst islands based on the topographic height, revealing a diameter distribution of 1.15 ± 0.40 nm. Based on SEM image and AFM, we can clearly say that the as-grown nanotubes are highly aligned with relatively narrow diameter distribution.

To further characterize the produced nanotubes, we measured Raman spectra of the individual nanotubes in the region between two catalyst islands or two metal contacts shown in Fig. 1(a). The nanotubes on quartz were characterized in terms of their metallic to semiconducting ratio using a micro-Raman system (100× objective with numer-

*E-mail address: chongwuz@usc.edu

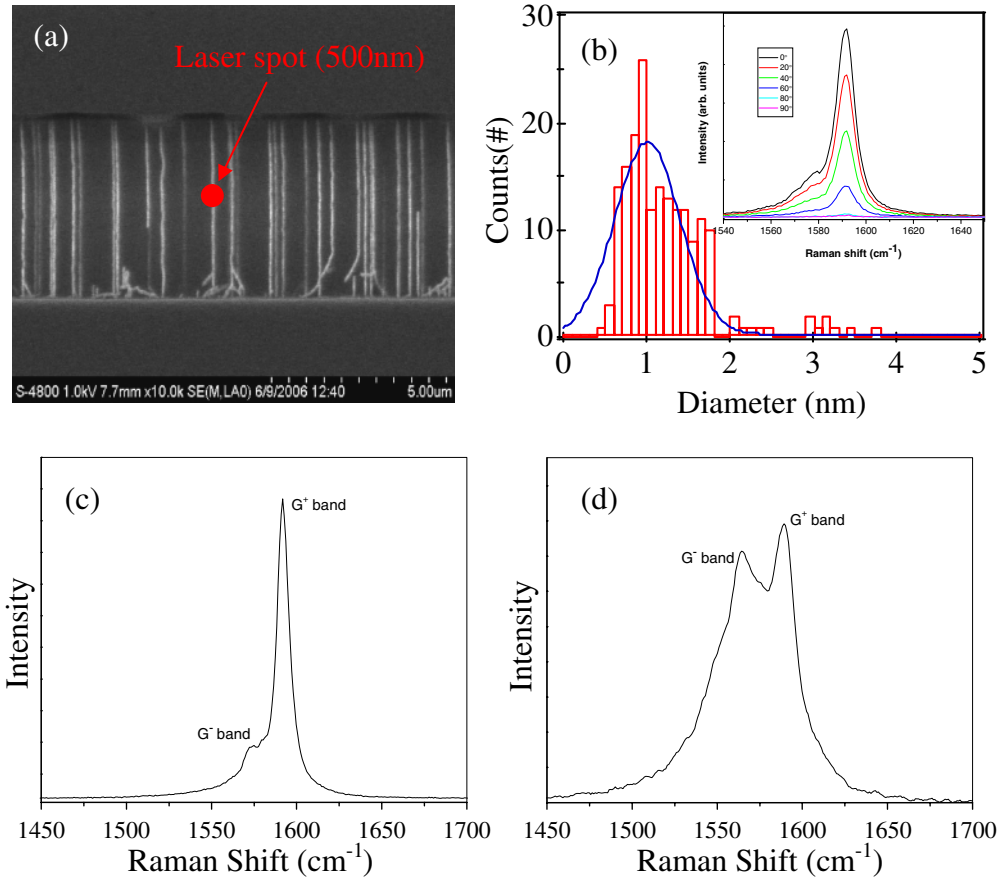

Fig. 1. (Color online) Detailed characterization of aligned carbon nanotubes. (a) SEM image of aligned nanotubes between source and drain electrodes, where the red dot stands for laser spot with 0.5 μm in diameter. (b) Histogram of diameter distribution of as-synthesized nanotubes. Inset: G band intensity as a function of the angle of polarization for an individual nanotube. (c) Typical Raman spectrum of semiconducting SWNTs characterized as Lorentzian lineshape. (d) Typical Raman spectrum of metallic SWNTs characterized as Breit–Wigner–Fano (BWF) lineshape.

ical aperture of 0.95) equipped with three monochromatic sources with wavelengths of 532 nm, 633 nm, and near infrared 785 nm. By combining micro Raman spectroscopy and SEM, we were able to obtain accurate spectroscopic information at a single nanotube level throughout the device in Fig. 1(a), and Raman spectra were taken with a resolution of ~0.5 μm according to the numerical aperture employed. As a one-dimensional system, the excitation of normal vibration modes along the axis of aligned nanotubes exhibits a strong dependence on the linear polarization direction of the excitation source. Raman spectra of the aligned nanotubes were taken at random locations within the wavenumber region of 1540–1650 cm^{-1} at six different angles of incidence of the laser polarization plane with respect to the nanotubes principal axis. Inset of Fig. 1(b) shows a typical measurement of the C=C stretch (G band) intensity as a function of the angle of polarization. The Raman resonance is strongly suppressed when the light is polarized perpendicular to the nanotube axis. This result gives a good insight of the high degree of alignment of nanotubes. The electronic nature of aligned nanotubes is also revealed by analyzing the two most intense peaks in the tangential vibration mode (G^- and G^+ bands) and the RBM frequencies of the nanotubes sampled. The G^- band for semiconducting nanotubes [Fig. 1(c)] exhibited a typical Lorentzian lineshape while metallic nanotubes [Fig. 1(d)] showed a broadened Breit–Wigner–Fano (BWF) G^- lineshape due to the presence of free electrons in the conduction band.[14] A metallic to semiconducting ratio of 1 : 2.7 was determined by sampling 40 nanotubes. The result is summarized in Table I.

Table I. Metallic vs semiconducting nanotubes determined by Raman spectra.

	532 nm	633 nm	785 nm	Total
Metallic	5	2	4	11
Semiconductive	18	2	9	29
Total	23	4	13	40

Five nanotubes were missed by the Raman measurements.
Metallic nanotubes in sample: ~27.5%
Metallic to semiconducting ratio: ~1 : 2.7

The nanotube molecular structure is important in defining its electrical properties. In particular, defects can limit the mechanical and electrical properties of nanotubes, and the nanotube device performance as well. The disorder-induced Raman band (D band) is common to sp^2 hybridized disordered carbon materials,[16] which is activated in the presence of hetero-atoms, vacancies, or defects that lower the crystal symmetry of the infinite lattice.[17] The full width at half maximum (FWHM) of D band for the sampled nanotubes was measured to be ~20 cm^{-1} in average, indicating that the nanotubes are highly crystalline and that such a broad D band signal shows contribution from defects on the nanotube surface.[15]

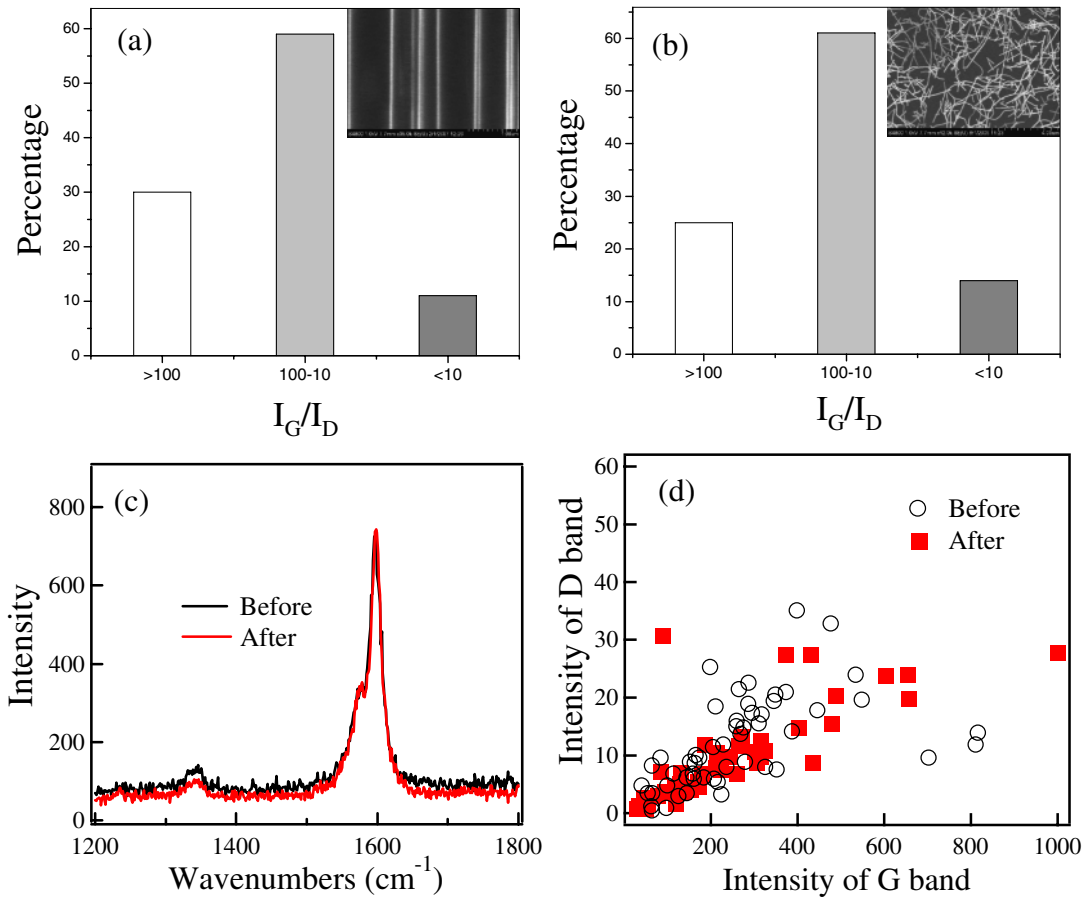

Fig. 2. (Color online) Defect analysis for aligned nanotubes on quartz (a) and randomly grown nanotubes on Si/SiO_2 (b). (c) Raman spectra of a nanotube before (black) and after (red) transfer, showing little difference. (d) Raman intensity of D- and G-bands of an ensemble of 60 nanotubes before and after transfer.

The ratio between the intensities of the G band and the disorder-induced D band (I_{G+}/I_D) is usually used to characterize the defect density of carbon nanotubes.[15] However, as the ratio I_{G+}/I_D depends on the excitation laser energy,[22] it is important to ascertain that the variation in I_{G+}/I_D observed for the nanotubes corresponds to differences in the defect density and not to different resonance conditions. Therefore, we employed only one excitation laser energy to characterize defect density in nanotubes, which eliminates the variation due to different laser energies. In addition, we only included in the analysis nanotubes that were in resonance with the excitation laser employed, in order to avoid variations due to different resonance conditions between the nanotubes studied. Following this approach, we characterized the defect density of approximately 60 resonant nanotubes (average diameter 1.15 nm), with an excitation source of 532 nm (2.33 eV), using the Raman intensity ratio I_{G+}/I_D.

I_{G+}/I_D ratio of less than 10 typically represents highly entangled, defective carbon nanotubes.[18] Figure 2(a) shows that only a small fraction of our nanotubes have a highly defective structure with I_{G+}/I_D less than 10. Besides, around 30% of the resonant nanotubes here have I_{G+}/I_D ratio higher than 10^2. This is comparable to a highly crystalline purified single-walled nanotube which shows a D band signal damping. On the other hand, 60% of the resonant nanotubes exhibited a low intensity D band with I_{G+}/I_D between 10 and 10^2. Almost the same trend is seen for the nanotubes synthesized on SiO_2 in Fig. 2(b), which indicates that the straight aligned carbon nanotubes grown on quartz have comparable defect density to those produced on SiO_2. Recently, a facile transfer process using Au film has been reported to easily transfer aligned nanotubes from the original quartz substrates to virtually any other substrates, and then fabricated nanotube devices.[10,11,19] In order to ascertain whether the transfer process induces defects in the nanotubes, we have taken Raman spectra from nanotubes before and after the transfer. Figure 2(c) shows the typical result from one nanotube, where little difference was observed, thus testifying to the high integrity of the transferred nanotubes. In addition, we characterized the defect density of approximately 60 nanotubes by comparing the Raman G and D line intensity. Figure 2(d) plots the distribution of the D and G band intensities for those nanotubes before and after the transfer process, and the majority of nanotubes exhibited very low D line intensity compared to G band intensity, indicating very good nanotube quality both before and after the transfer.

In order to investigate the transport properties of nanotube devices, we fabricated both top- and back-gated devices based on the as-grown aligned nanotubes and the transferred nanotubes, respectively. For the fabrication of nanotube transistors, we first used photolithography to define Pd source and drain electrodes with the channel width and length of 50

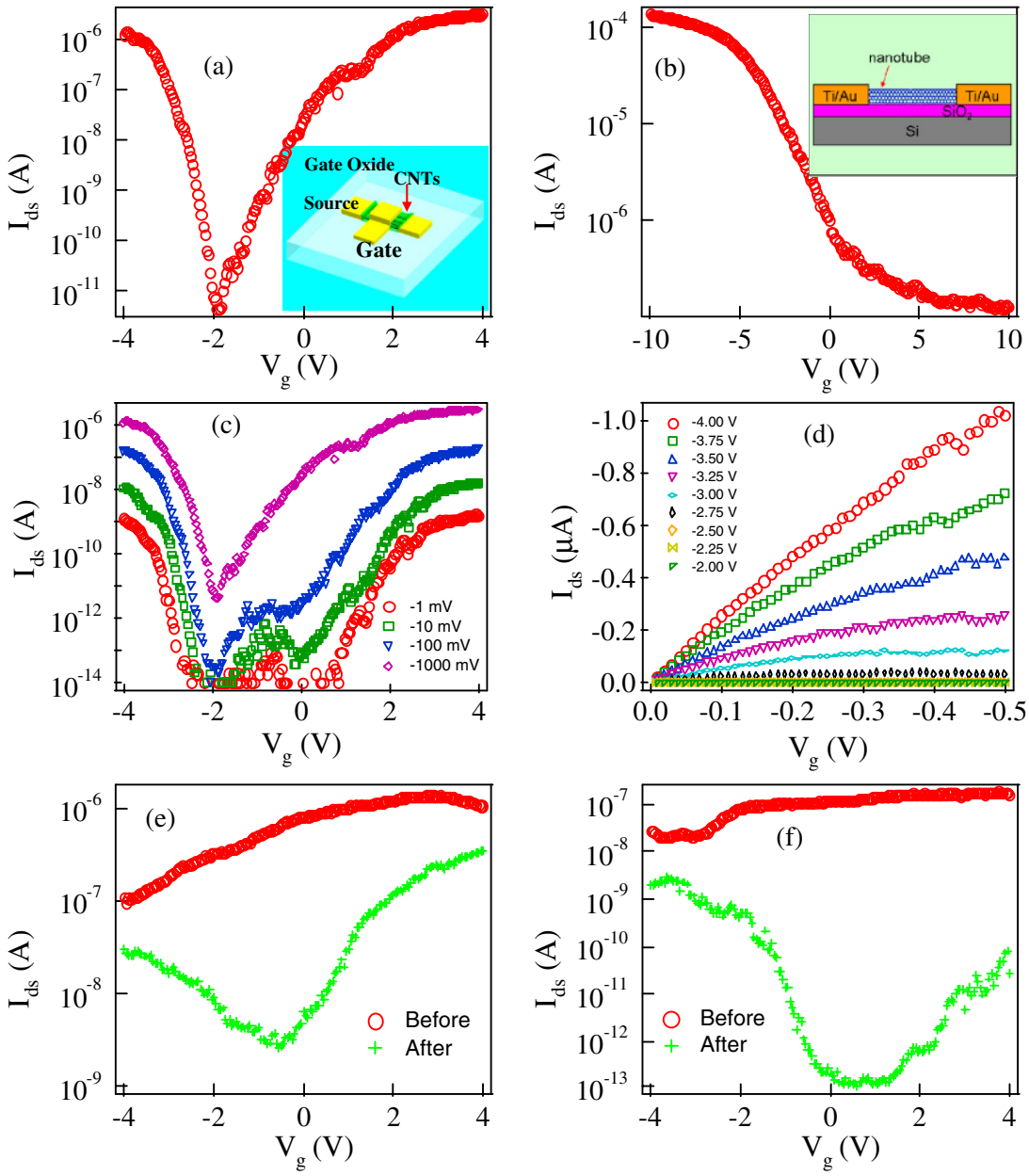

Fig. 3. (Color online) (a) I–V_g curve of a top-gated transistor exhibiting ambipolar behavior $V_{ds} = -1$ V. Inset: schematic diagram of device. (b) I–V_g curve of a back-gated transistor exhibiting p-type unipolar behavior $V_{ds} = -1$ V. Inset: schematic diagram of device. (c) A family of I–V_g curves at $V_{ds} = -1$, -10, -100, -1000 mV. (d) A family of I–V_{ds} curves at different gate voltages. (e, f) I–V_g curves for predominantly p- and n-type device, respectively.

and 4 μm, respectively, followed by O_2 plasma etching to remove unwanted nanotubes in the outside of active channel. For the top-gated devices, 20-nm HfO_2 was coated onto the samples as the gate dielectric by atomic layer deposition (ALD), and then Ti/Au top-gate electrodes were defined by photolithography. Both top- and back-gated device structures are shown in the inset of Figs. 3(a) and 3(b), respectively. Figure 3(a) displays the current versus gate voltage (I–V_g) curve of a top-gated device showing pronounced ambipolar transport at room temperature with $V_{ds} = -1$ V, showing p-type behavior for $V_g < -2.6$ V and n-type behavior for $V_g > 0$ V. The transconductance of this device can be derived to be 2.16 μS in the p region and 0.78 μS in the n region. We can also extract the subthreshold swing of this device as 110 mV/decade in the p region and 300 mV/decade in the n region, respectively. To clearly resolve the subthreshold regions at different drain voltages, we plotted a family of I–V_g curves at different source–drain voltages of -1, -10, -100, and -1000 mV in Fig. 3(c). One can see that the on/off ratio is as high as 10^7 at $V_{ds} = -100$ mV. At the small source–drain voltage (-1 mV), the I–V_g curve shows a broad valley between -2.5 to 1 V, indicating a large band gap.[20] The seemingly flat valley observed in Fig. 3(c) at low V_{ds} ($V_{ds} = -1$ mV) between $V_g = -2.4$ to 0.8 V can be correlated with the energy gap (E_g) of the nanotubes. E_g for nanotubes with diameter around 1.15 nm would be 0.6 eV, and the gate efficiency (α) of our devices can be estimated to be $\alpha = E_g/\Delta V_g \sim 0.2$. Considering the dielectric thickness of 20 nm HfO_2 used for our devices, this value of $\alpha \sim 0.2$ agrees well with values reported in the literature for similar top-gated nanotube transistors, such as a value of $\alpha \sim 0.6$ for devices with 8 nm HfO_2 gate dielectric.[23]

In addition, Fig. 3(d) shows a family of I–V_{ds} curves at different gate voltages in the p-region. The curves at gate voltages from −4 to −2.75 V are well separated with current saturation at higher source–drain voltage, while the curves at gate voltages from −2.50 to 2.00 V are almost overlapped to each other with very small current, which indicates that the gate threshold voltage is around −2.50 V. In contrast to the top-gated devices covered with HfO_2 layer, the back-gated devices with the transferred nanotubes showed p-type unipolar transport characteristics [Fig. 3(b)] due to the doping effect from moisture and O_2 in the air. In particular, the ambipolar behavior in the top-gated devices can be used for the polarity control of the transistor to get a predominant either p- or n-type one.

It is well known that the nanotube transistors with metallic nanotubes are not depletable with on/off ratio normally less than 10 due to the presence of metallic nanotubes in the conduction channels. On the other hand, these devices have a large amount of semiconducting nanotubes in the channel, which are different in the threshold voltage and band gap due to the doping and diameter variation, respectively. Therefore, out of the large population of nanotubes in the conduction channel, we could sort out one or some nanotubes with only n- or p-type behavior within a certain range of gate voltage sweeping controllably. To obtain the n- or p-type transistor, electrical breakdown was performed by sweeping source–drain voltage from 0 V while keeping gate voltage at $V_g = -5$ or 5 V, respectively. After each breakdown, we need to measure the gate transfer curve to check the on/off ratio and gate dependence. This breakdown process can happen for several times until we got good gate dependence with on/off ratio larger than 100. After the breakdown, one device shows predominately n-type behavior with significant improvement of on/off ratio (from 5 to 100) compared to that before any breakdown [Fig. 3(e)], while the other shows predominately p-type behavior with on/off ratio of 10^4 and one order of magnitude conductance reduction [Fig. 3(f)]. We found that the electrical breakdown process with different gate polarity (here, −5 or +5 V) can reproducibly lead to a transistor with predominately n- or p-type behavior based on the top-gated devices. It is believed that nanotubes with significant p-channel (n-channel) conductance enhanced by negative (positive) gate voltage were likely to be first removed together with metallic nanotubes, leaving predominately n-type (p-type) nanotubes untouched, during electrical breakdown. This approach can be used to build up the complementary nanotube circuits based on novel nanotube-on-insulator (NOI) approach.

3. Conclusions

In summary, the detailed characterization of aligned nanotube arrays have been performed by AFM and Raman microscopy in terms of diameter distribution, Raman polarization, defect analysis and the determination of metallic/semiconducting nanotube ratio. We found that the aligned nanotubes on quartz have a comparable or slightly better quality than the randomly grown nanotubes on Si/SiO_2 substrates, and metallic/semiconducting ratio is 1 : 2.7. In addition, we have fabricated top- and back-gated nanotube devices, which showed different electrical characteristics. Moreover, we have demonstrated a way to produce both predominate n- and p-type top-gated nanotube transistors by controlling the polarity of gate voltage during electrical breakdown. This will render us a way to build up complementary nanotube circuits based on NOI platform.

Acknowledgements

We gratefully acknowledge support from a NSF CAREER Award, a NSF-CENS grant, and a SRC MARCO/DARPA grant and MARCO/FENA center.

1) S. Ijima: Nature **354** (1991) 56.
2) M. S. Dresselhaus, G. Dresselhaus, and Ph. Avouris: *Carbon Nanotubes: Synthesis, Structure, Properties, and Applications* (Springer, New York, 2001).
3) A. Ismach, L. Segev, E. Wachtel, and E. Joselevich: Angew. Chem., Int. Ed. **43** (2004) 6140.
4) S. Han, X. Liu, and C. Zhou: J. Am. Chem. Soc. **127** (2005) 5294.
5) H. Ago, K. Nakamura, K. Ikeda, N. Uehara, N. Ishigami, and M. Tsuji: Chem. Phys. Lett. **408** (2005) 433.
6) C. Kocabas, S. Hur, A. Gaur, M. A. Meitl, M. Shim, and J. A. Rogers: Small **1** (2005) 1110.
7) K. Ryu, A. Badmaev, L. Gomez, F. Ishikawa, B. Lei, and C. Zhou: J. Am. Chem. Soc. **129** (2007) 10104.
8) L. Ding, D. Yuan, and J. Liu: J. Am. Chem. Soc. **130** (2008) 5428.
9) X. Liu, S. Han, and C. Zhou: Nano Lett. **6** (2006) 34.
10) S. J. Kang, T. Ozel, M. Shim, N. Pimparkar, M. A. Alam, S. V. Rotkin, and J. A. Rogers: Nat. Nanotechnol. **2** (2007) 230.
11) K. Ryu, A. Badmaev, C. Wang, A. Lin, N. Patil, L. Gomez, A. Kumar, S. Mitra, H. S. P. Wong, and C. Zhou: Nano Lett. **9** (2009) 189.
12) G. Xu, F. Liu, S. Han, K. Ryu, A. Badmaev, B. Lei, C. Zhou, and K. Wang: Appl. Phys. Lett. **92** (2008) 223114.
13) C. Kocabas, M. Shim, and J. A. Rogers: J. Am. Chem. Soc. **128** (2006) 4540.
14) J. Kong, H. T. Soh, A. M. Cassell, C. F. Quate, and H. Dai: Nature **395** (1998) 878.
15) M. A. Pinenta, A. Marucci, S. A. Empedocles, M. G. Bowendi, E. B. Hanlon, A. M. Rao, P. C. Eklund, R. E. Smally, G. Dresselhaus, and M. S. Dresselhaus: Phys. Rev. B **58** (1998) 16016.
16) A. Dillon, P. Parilla, J. Alleman, T. Gennett, K. Jones, and M. Heben: Chem. Phys. Lett. **401** (2005) 522.
17) M. Pimenta, A. Jorio, S. Brown, A. Souza Filho, G. Dresselhaus, J. Hafner, C. Lieber, R. Saito, and M. Dresselhaus: Phys. Rev. B **64** (2001) 041401.
18) A. Filho, A. Jorio, G. Samsonidze, G. Dresselhaus, R. Saito, and M. S. Dresselhaus: Nanotechnology **14** (2003) 1130.
19) S. Kim, V. Park, E. Ra, K. Kim, K. An, Y. Lee, J. Choi, C. Park, S. Doo, M. Park, and C. Yang: Appl. Phys. Lett. **90** (2007) 023114.
20) F. N. Ishikawa, H. Chang, K. Ryu, P. Chen, A. Badmaev, L. Gomez, G. Shen, and C. Zhou: ACS Nano **3** (2009) 73.
21) W. Kim, H. C. Choi, M. Shim, Y. Li, D. Wang, and H. Dai: Nano Lett. **2** (2002) 703.
22) L. G. Cancado, A. Jorio, and M. A. Pimenta: Phys. Rev. B **76** (2007) 064304.
23) A. Javey, J. Guo, D. B. Farmer, Q. Wang, E. Yenilmez, R. G. Gordon, M. Lundstrom, and H. Dai: Nano Lett. **4** (2004) 1319.